Preparation and Biological Evaluation of ^{64}Cu-CB-TE2A-sst$_2$-ANT, a Somatostatin Antagonist for PET Imaging of Somatostatin Receptor–Positive Tumors

Thaddeus J. Wadas, Martin Eiblmaier, Alexander Zheleznyak, Christopher D. Sherman, Riccardo Ferdani, Kexian Liang, Samuel Achilefu, and Carolyn J. Anderson

Mallinckrodt Institute of Radiology, Washington University School of Medicine, St. Louis, Missouri

Recently, the somatostatin receptor subtype 2 (SSTR2) selective antagonist sst$_2$-ANT was determined to have a high affinity for SSTR2. Additionally, ^{111}In-1,4,7,10-tetraazacyclododecane-1,4,7,10-tetraacetic acid-sst$_2$-ANT showed high uptake in an SSTR2-transfected, tumor-bearing mouse model and suggested that radiolabeled SSTR2 antagonists may be superior to agonists for imaging SSTR2-positive tumors. This report describes the synthesis and evaluation of ^{64}Cu-CB-4,11-bis(carboxymethyl)-1,4,8,11-tetraazabicyclo[6.6.2]hexadecane-sst$_2$-ANT (^{64}Cu-CB-TE2A-sst$_2$-ANT) as a PET radiopharmaceutical for the in vivo imaging of SSTR2-positive tumors. **Methods:** Receptor-binding studies were performed to determine the dissociation constant of the radiopharmaceutical ^{64}Cu-CB-TE2A-sst$_2$-ANT using AR42J rat pancreatic tumor cell membranes. The internalization of ^{64}Cu-CB-TE2A-sst$_2$-ANT was compared with that of the ^{64}Cu-labeled agonist ^{64}Cu-CB-TE2A-tyrosine^3-octreotate (^{64}Cu-CB-TE2A-Y3-TATE) in AR42J cells. Both radiopharmaceuticals were also compared in vivo through biodistribution studies using healthy rats bearing AR42J tumors, and small-animal PET/CT of ^{64}Cu-CB-TE2A-sst$_2$-ANT was performed. **Results:** The dissociation constant value for the radiopharmaceutical was determined to be 26 ± 2.4 nM, and the maximum number of binding sites was 23,000 fmol/mg. ^{64}Cu-CB-TE2A-sst$_2$-ANT showed significantly less internalization than did ^{64}Cu-CB-TE2A-Y3-TATE at time points from 15 min to 4 h. Biodistribution studies revealed that the clearance of ^{64}Cu-CB-TE2A-sst$_2$-ANT from the blood was rapid, whereas the clearance of ^{64}Cu-CB-TE2A-sst$_2$-ANT from the liver and kidneys was more modest at all time points. Tumor-to-blood and tumor-to-muscle ratios were determined to be better for ^{64}Cu-CB-TE2A-sst$_2$-ANT than those for ^{64}Cu-CB-TE2A-Y3-TATE at the later time points, although liver and kidney uptake was significantly higher. Small-animal imaging using ^{64}Cu-CB-TE2A-sst$_2$-ANT revealed excellent tumor-to-background contrast at 4 h after injection, and standardized uptake values remained high even after 24 h. **Conclusion:** The PET radiopharmaceutical ^{64}Cu-CB-TE2A-sst$_2$-ANT is an attractive agent, worthy of future study as a PET radiopharmaceutical for the imaging of somatostatin receptor–positive tumors.

Key Words: ^{64}Cu; somatostatin; antagonist

J Nucl Med 2008; 49:1819–1827
DOI: 10.2967/jnumed.108.054502

Radiolabeled somatostatin analogs have become important agents for molecular imaging and targeted radiotherapy of somatostatin receptor–positive tumors. Somatostatin analogs such as octreotide, octreotate, and tyrosine^3-octreotate (Y3-TATE) have been radiolabeled with ^{18}F and ^{124}I directly or conjugated to a bifunctional chelator for radiolabeling with metal radionuclides (*1–3*). Moreover, they have also been modified at the carboxy and amino termini to create multimodal imaging agents that can be used for PET, SPECT, and planar optical imaging (*4*).

Recently, Ginj et al. compared somatostatin receptor agonists and antagonists as targeting ligands and their specific affinity for the 5 different subtypes of the somatostatin receptor (*5*). The somatostatin receptor subtype 2 (SSTR2) selective antagonist sst$_2$-ANT was determined to have a high affinity for the SSTR2 receptor, which was not decreased by the presence of the conjugated chelator 1,4,7,10-tetraazacyclododecane-1,4,7,10-tetraacetic acid (DOTA) or a conjugated ^{nat}In-DOTA complex. Internalization of the SSTR2 was not observed using immunofluorescence internalization assays, even when the concentration of the antagonist exceeded 9 μM. Biodistribution studies using ^{111}In-DOTA-sst$_2$-ANT revealed high uptake and a slow clearance of the radiopharmaceutical in nude mice bearing tumors comprising human embryonic kidney (HEK) cells that were stably transfected to express only SSTR2.

Although ^{111}In-DOTA-sst$_2$-ANT shows promise as a radiotracer for SPECT, DOTA-sst$_2$-ANT has not been evaluated as a PET radiopharmaceutical labeled with other M^{2+} or M^{3+} radiometals such as ^{64}Cu, ^{68}Ga, or ^{86}Y. In the case of ^{64}Cu, the imaging properties are expected to be suboptimal

Received May 20, 2008; revision accepted Jul. 14, 2008.
For correspondence or reprints contact: Carolyn J. Anderson, Mallinckrodt Institute of Radiology, Washington University School of Medicine, 510 S. Kingshighway Blvd., Campus Box 8225, St. Louis, MO 63110.
E-mail: andersoncj@wustl.edu

because of the reputation of DOTA as an indiscriminate metal chelator and the kinetic lability of the radiometal complexes (*6*). Although the latter factor contributes to greater radiometal transchelation to cellular proteins, both factors have been shown to reduce image quality and adversely affect the imaging results.

Over the last decade, Weisman and Wong and others have synthesized and studied several new bridged tetraazamacrocyclic chelators and their transition metal complexes (*7,8*). These ligands use an ethylene bridge between nonadjacent nitrogens located on the tetraazamacrocycle and have been synthesized with carboxymethyl arms to fully envelop the cation in an octahedral geometry and neutralize the dicationic charge of the metal center. In addition, several reports exist that demonstrate superior stability of these ^{64}Cu complexes in vivo when compared with ^{64}Cu complexes formed with traditional chelators such as DOTA and 1,4,8,11-tetraazacyclo-dodecane-1,4,8,11-tetraacetic acid (*9*). This enhanced stability was retained even after conjugation to the peptide Y3-TATE (*10*). This study sought to combine the enhanced binding properties of the sst$_2$-ANT peptide with the ultrastable ^{64}Cu chelator 4,11-bis(carboxymethyl)-1,4,8,11-tetraazabicyclo[6.6.2]hexadecane (CB-TE2A) (Fig. 1) to determine its usefulness as a PET radiopharmaceutical for the in vivo imaging of SSTR2-positive tumors.

MATERIALS AND METHODS

^{64}Cu (half-life, 12.7 h; β^+, 17.8%, $E_{\beta+max}$, 656 keV; β^-, 38.4%, $E_{\beta-max}$, 573 keV) (*11*) was produced on a CS-15 biomedical cyclotron at Washington University School of Medicine (*12*). All other chemicals were purchased from Sigma-Aldrich Chemical Co., and solutions were prepared using ultrapure water (resistivity, 18 MΩ cm). The peptide Y3-TATE was prepared by standard literature protocols (*13*), and CB-TE2A and ^{64}Cu-CB-TE2A-Y3-TATE were prepared according to literature procedures (*8, 10*). Radiochemistry reaction progress and purity were monitored by analytic reversed-phase high-performance liquid chromatography (HPLC), which was performed on a chromatography system (600E; Waters) with a photodiode array detector (991; Waters) and a radioactivity detector (Ortec, model 661; EG&G Instruments). A C-18 column (Vydak) was used with a gradient that changed from 0.1% trifluoroacetic acid (TFA) in water to a concentration of 60:40 0.1% TFA/Water:0.1% TFA/CH_3CN over the course of 15 min. In addition, radio–thin-layer chromatography (radio-TLC) was conducted on an AR scanner (Bioscan) equipped with a concentration of 10% methane:argon gas supply and a PC interface running analysis software (Winscan, version 3; Academic Software). C-18 plates with an eluent mixture of 3:7 10% NH_4OAc:MeOH and the complex $^{64}Cu(OAc)_2$ as a standard control were used. Radioactive samples were counted using an automated well-type γ-counter (8000; Beckman) or a β-plate reader (1450 Micro Beta; Perkin Elmer). The PET data were acquired using either a microPET Focus 120 or a microPET Focus 220 (Siemens Medical Solutions), and the CT data were collected using a microCAT II (Siemens Medical Solutions).

Male Lewis rats (age, 21 d; weight, 40–50 g) were purchased from Charles River Laboratories and handled according to the procedures outlined by the Washington University Animal Studies Committee. AR42J pancreatic tumors were implanted into the hind limbs by serial passage as previously described and were allowed to grow 10–14 d, after which time tumors achieved a solid palpable mass (*10*).

Synthesis of CB-TE2A-sst$_2$-ANT

The peptide CB-TE2A-Phe(4-NO_2)-cyclo(D-Cys-Tyr-D-Trp-Lys-Thr-Cys)-DTyr-NH_2 was synthesized on a 30 μM scale by standard Fmoc solid-phase peptide synthesis, as reported previously (*14*). The peptide was assembled on a Rink Amide resin starting with Fmoc-D-Tyr. The coupling of subsequent Fmoc-protected amino acids (90 μmol each) was achieved by activating the carboxyl group with a 1:1 mixture of *N*-hydroxylbenzotriazole (90 μmol) and 2-(^{1}H benzotriazole-1-yl)-1,1,1,3-tetramethyluronium hexafluorophosphate (90 μmol) and *N,N*-diisopropylethylamine (DIEA; 180 μmol). Disulfide cyclization was achieved with thallium trifluoroacetate (27.6 mg, 50.4 μmol) in anhydrous dimethylformamide (1 mL), and CB-TE2A (90 μmol) was incorporated

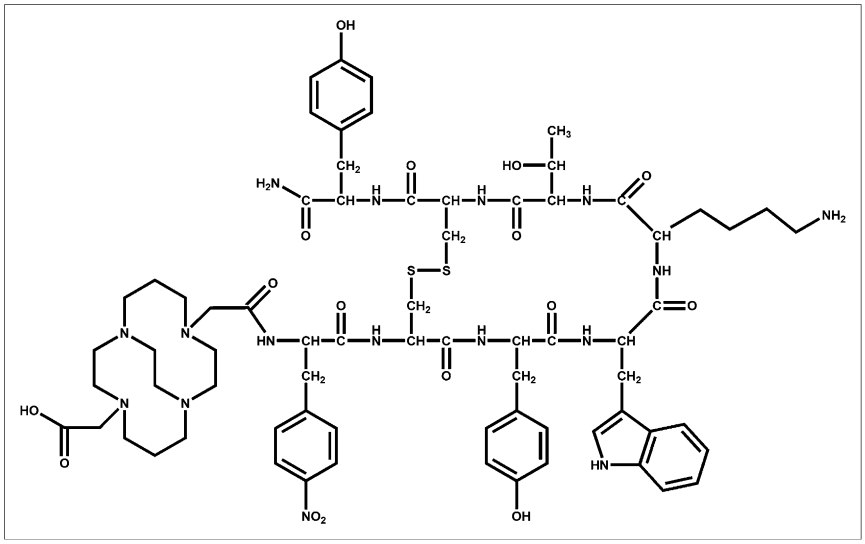

FIGURE 1. Structure of unlabeled peptide chelator conjugate CB-TE2A-sst$_2$-ANT.

at the N-terminus of the peptide by activating the acid with dicyclohexylcarbodiimide (120 μmol) and DIEA (120 μmol). Cleavage of the peptide from resin and HPLC purification were performed as described previously (*14*). HPLC purification was performed on a protein and peptide C-18 column (22 × 250 mm, 5 μm; Vydac) at a flow rate of 10 mL/min. Flow A was 0.1% TFA in water, and flow B was 0.1% TFA in acetonitrile. The elution method for purification started with a linear gradient from 90% to 70% A over 10 min, followed by 70% to 50% A for 10 min, and then from 50% to 35% A for 10 min. The elution profile was monitored by ultraviolet absorbance at 214 nm.

The CB-TE2A-sst_2-ANT was obtained as a white powder (12 mg, 8 μmol) after lyophilization in a 3:1 H_2O:acetonitrile mixture. Analytic HPLC was performed on a Vydac protein and peptide C-18 column (100 × 4.6 mm, 5 μm) at a flow rate of 1 mL/min. Flow A was 0.1% TFA in water, and flow B was 0.1% TFA in acetonitrile. The elution method for analytic HPLC started with a linear gradient from 90% to 40% A over 5 min, followed by 40% to 25% A for 2 min, and the elution profile was monitored by ultraviolet absorbance at 214 nm. The peptide was also characterized by electrospray mass spectrometry. Calculated mass, 1,479.0; (ESI+MS) m/z (% relative intensity, ion), 1,479.80 (5, M+1), 740.20 (100, M+2).

A similar procedure was used to prepare and purify the control peptide AC-Phe(4-NO_2)-cyclo(D-Cys-Tyr-D-Trp-Lys-Thr-Cys)-DTyr-NH_2 (10 mg, 7 μmol), except that acetic anhydride was used to cap the N-terminal amino group. HPLC purification was performed as described above. The elution method for purification started with a linear gradient from 90% to 75% A over 10 min, followed by 75% to 65% A for 15 min, and then 65% to 55% A for 10 min; the elution profile was monitored by ultraviolet absorbance at 214 nm. Analytic HPLC was performed as previously described, and electrospray mass spectrometry also was performed. Calculated mass, 1,197.60; (ESI+MS) m/z (% relative intensity, ion), 1,196.85 (100, M+1).

Radiochemistry

The complexation of ^{64}Cu to CB-TE2A-sst_2-ANT was achieved by reacting 1 μg (6.3×10^{-4} μmol) of CB-TE2A-sst_2-ANT, 118 μL of 0.1 M NH_4OAc (pH, 8.0), and 37 MBq of $^{64}CuCl_2$ in 0.1N hydrochloric acid for 1.5 h at 95°C. The reaction was further purified using a previously published method (*15*). Purity after purification was greater than 95% based on radio-TLC and radio-HPLC analysis.

Receptor-Binding Studies

AR42J cell membrane preparations were used for binding assays, and assays were performed on a 96-well filtration plate (Multiscreen Durapore; Millipore) using previously described methods, with some modifications (*16*). Membranes were diluted in binding buffer (50 mM Tris-hydrochloride [pH, 7.4]; 5 mM $MgCl_2 \cdot 6\ H_2O$; 0.1% bovine serum albumin; and 0.5 μg of aprotinin, 200 μg of bacitracin, 10 μg of leupeptin, and 10 μg of pepstatin A per milliliter), and 20 μg of membrane protein were used per well. Increasing concentrations of ^{64}Cu-CB-TE2A-sst_2-ANT were added to membranes to measure total binding, and unspecific binding was determined by conducting the assay in the presence of an excess of CB-TE2A-sst_2-ANT. After incubation of the membranes at room temperature for 2 h, the medium was removed and the membranes were washed twice with 200 μL of binding buffer. OptiPhase Super-Mix (50 μL; PerkinElmer) was added to each well, and bound activity was measured with a liquid scintillation and luminescence counter (1450 Microbeta; Perkin Elmer). All dissociation constant (K_d) values were estimated from nonlinear curve fitting of bound peptide versus the sum of the concentrations of ^{64}Cu- and CB-TE2A-sst_2-ANT using software (Prism; GraphPad).

Internalization Studies

AR42J cells were cultured in Iscove's Dulbecco/Vogt modified Eagle's minimal essential medium (DMEM) supplemented with 10% fetal bovine serum; cells were incubated at 37°C in a humidified 5% CO_2 atmosphere. Before each assay, cells were harvested with a rubber-tipped scraper (Sarstedt, Inc.), washed twice with phosphate-buffered saline, and resuspended in Iscove's DMEM supplemented with 10% fetal bovine serum at 1×10^6 cells per 500 μL. Aliquots of cell suspension (500 μL) were placed in 1.7-mL microfuge tubes (Midwest Scientific). ^{64}Cu-CB-TE2A-sst_2-ANT (specific activity, 8.5 MBq/μg) or ^{64}Cu-CB-TE2A-Y3-TATE (specific activity, 8.5 MBq/μg) was added to each tube, to a final concentration of 4.0 nM for each radiotracer. The tubes were incubated at 37°C, with rotation. To block specific binding at each time point, tubes containing 500-μL cell suspensions (1×10^6 cells/500 μL) were incubated 5 min at room temperature with 2 μg of Y3-TATE or 2 μg of sst_2-ANT. At each time point, surface-bound fractions were collected as previously described (*17*). Internalized radioactivity was collected by lysing the cells in 0.5% sodium dodecyl sulfate. Total protein concentration in the cell lysate was determined using the BCA Protein Assay (Pierce Biotechnology). Internalized and surface-bound fractions were expressed as counts/min/mg of protein.

Biodistribution

The biodistribution study was conducted as previously described (*18*). Briefly, healthy male Lewis rats (39 d old) bearing AR42J tumors were injected with ^{64}Cu-CB-TE2A-sst_2-ANT (0.74 MBq, 40 ng in 150 μL/rat) or ^{64}Cu-CB-TE2A-Y3-TATE (0.74 MBq, 25 ng in 150 μL/rat) via the tail vein. Animals were sacrificed at selected time points after injection, and organs of interest were removed, weighed, and counted on a γ-counter (8000; Beckman). Blocking studies were also performed using healthy male Lewis rats (39 d old) bearing AR42J tumors to examine in vivo uptake specificity. ^{64}Cu-CB-TE2A-sst_2-ANT (0.74 MBq, 40 ng in 150 μL/rat) was coinjected with 175 μg of sst_2-ANT via the tail vein, or ^{64}Cu-CB-TE2A-Y3-TATE (0.74 MBq, 25 ng in 150 μL/rat) was coinjected with 175 μg of Y3-TATE via the tail vein. The percentage injected dose per gram and percentage injected dose per organ were calculated by comparing them with a weighed, counted standard.

Imaging Using Small-Animal PET/CT

Imaging studies were performed with male Lewis rats bearing AR42J tumors in both hind limbs. Four rats were injected with ^{64}Cu-CB-TE2A-sst_2-ANT (13 MBq, 740 ng in 150 μL/rat). At 1, 4, and 24 h after injection, rats were anesthetized with 1–2% isoflurane and imaged. Blocking studies were also performed at 4 h. A separate set of 4 male Lewis rats bearing AR42J tumors in their hind limbs were coinjected via the tail vein with ^{64}Cu-CB-TE2A-sst_2-ANT (9.8 MBq, 550 ng in 150 μL/rat) and 1,000 μg of sst_2-ANT. For both groups and at all time points, standardized uptake values (SUVs) were determined using the formula SUV = ([nCi/mL] × [animal weight (g)]/injected dose [nCi]).

Statistical Methods

All of the data are presented as mean ± SD or mean followed by 95% confidence interval (CI) in parentheses. For statistical classification, a Student *t* test (2-tailed, unpaired) was performed using Prism software (GraphPad). Any *P* value less than 0.05 was considered significant.

RESULTS

Synthesis of Peptides and CB-TE2A Conjugate

All peptides used in this study were prepared by standard Fmoc peptide chemistry. Disulphide cyclization and peptide purification were performed as reported elsewhere (*14*). Pretreatment of CB-TE2A with dicyclohexylcarbodiimide appears to form an acid anhydride from the dicarboxylic acid function, which then reacts selectively with the N-terminal amino group of the peptide on solid support. The desired compound was obtained in 26% yield, and the presence of a cross-linked peptide was not observed, demonstrating the advantage of the solid-phase synthesis approach over reactions in solution. Previous studies have shown that a similar chelating group that possesses 2 reactive carboxylic acid groups (tri-*t*-butyl-diethylenetriaminepentaacetic acid [DTPA]) forms predominantly a monopeptide conjugate on solid support (*13*). The excellent stability of CB-TE2A under the TFA peptide cleavage condition facilitates the automation of the synthesis protocol.

Radiochemistry

The preparation of ^{64}Cu-CB-TE2A-sst$_2$-ANT was performed using a previously described method (*15*). Radiochemical purity was between 60% and 99% after the reaction was heated. In those reactions of the highest purity (≥95%), only 1 peak (R_f of 0.6) was observed by radio-TLC, which was attributed to the expected radiopharmaceutical product. This result was validated using radio-HPLC, in which only 1 product peak was observed with a retention time of 15.5 ± 0.5 min. The presence of $^{64}Cu(OAc)_2$ at the origin ($R_f = 0$) of the TLC plate or in void volume of the HPLC run (retention time = 1–2 min) was negligible, indicating that nonchelated ^{64}Cu was not present in the reaction and the formation of the complex was complete.

For reactions of less than 95% purity due to nonchelated ^{64}Cu, the reaction was purified using ethylenediaminetetraacetic acid (EDTA) and a C-18 SepPak Light cartridge (Waters). A buffered EDTA solution was added to chelate any ^{64}Cu not already incorporated into the ligand. A total of 75% of the radiolabeled product was eluted from the cartridge using absolute ethanol containing 0.5% acetic acid. Concentration using a vacuum concentrator did not cause significant degradation to the radiopharmaceutical, and after redilution in a suitable buffer or saline the radiopharmaceutical demonstrated sufficient purity to be used for further studies with cells and animals. ^{64}Cu-CB-TE2A-sst$_2$-ANT was obtained at a purity of greater than 95% and a specific activity range of 13–37 MBq/μg using this method.

Receptor-Binding and Cellular Internalization Studies

A saturation binding assay was performed with AR42J tumor cell membranes bearing SST receptors, using previously described procedures that were slightly modified (Fig. 2) (*16*). The K_d value for the radiopharmaceutical was determined to be 26 ± 2.4 nM (21.72–31.17 nM) and the maximum number of binding sites (B_{max}) was 23,000 fmol/mg (21,052–24,893 fmol/mg), demonstrating that ^{64}Cu-CB-TE2A-sst$_2$-ANT had a significantly lower affinity for SSTR2 than was observed for ^{64}Cu-CB-TE2A-Y3-TATE (K_d, 1.7 nM). However, ^{64}Cu-CB-TE2A-sst$_2$-ANT binds to 14-fold more SSTR sites than does the agonist (B_{max} for the agonist vs. antagonist, 1,596 fmol/mg vs. 23,000 fmol/mg) on the tumor cell membrane.

Internalization studies were also performed using AR42J tumor cells (Fig. 3). The nonzero *y*-intercept for both the agonist and antagonist suggests a rapid early internalization phase at 15 min, followed by a slower phase at 30 min. Data after 30 min showed no significant change in radiotracer internalization. Although it was expected that there would be either minimal or no internalization of ^{64}Cu-CB-TE2A-sst$_2$-ANT, there were significant levels of internalized agent (10-fold less at 15 and 30 min for ^{64}Cu-CB-TE2A-sst$_2$-ANT than for ^{64}Cu-CB-TE2A-Y3-TATE, however). In both cases, addition of the cold peptides (sst$_2$-ANT or Y3-TATE), along with the respective radiotracer to the cell suspensions, inhibited the internalization of either radiopharmaceutical. The surface-bound fraction of ^{64}Cu-CB-TE2A-sst$_2$-ANT was significantly greater than that of ^{64}Cu-CB-TE2A-Y3-TATE between 30 and 240 min.

Biodistribution Studies

Biodistribution studies of ^{64}Cu-CB-sst$_2$-ANT and ^{64}Cu-CB-TE2A-Y3-TATE were conducted on 39-d-old AR42J tumor–bearing male Lewis rats. The results of those studies are depicted in Figure 4. ^{64}Cu-CB-TE2A-Y3-TATE showed rapid blood clearance at 1 h, and by 24 h 74% of the activity present at 1 h was removed from the blood (Supplemental Table 1; supplemental materials are available online only at

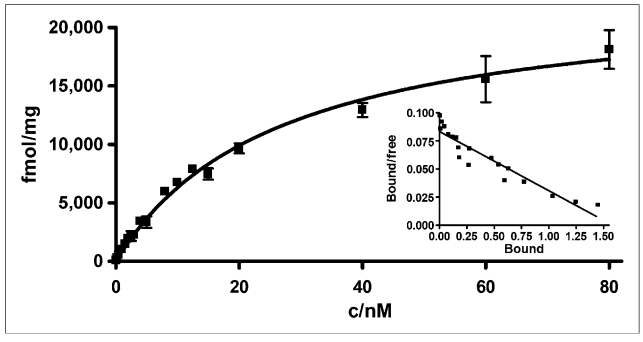

FIGURE 2. In vitro binding affinity of ^{64}Cu-CB-TE2A-sst$_2$-ANT for SSTR harvested from AR42J rat pancreatic tumor cell membranes was determined using saturation binding assay. K_d of radiopharmaceutical was determined to be 26 ± 2.4 nM, and B_{max} was determined to be 23,000 fmol/mg.

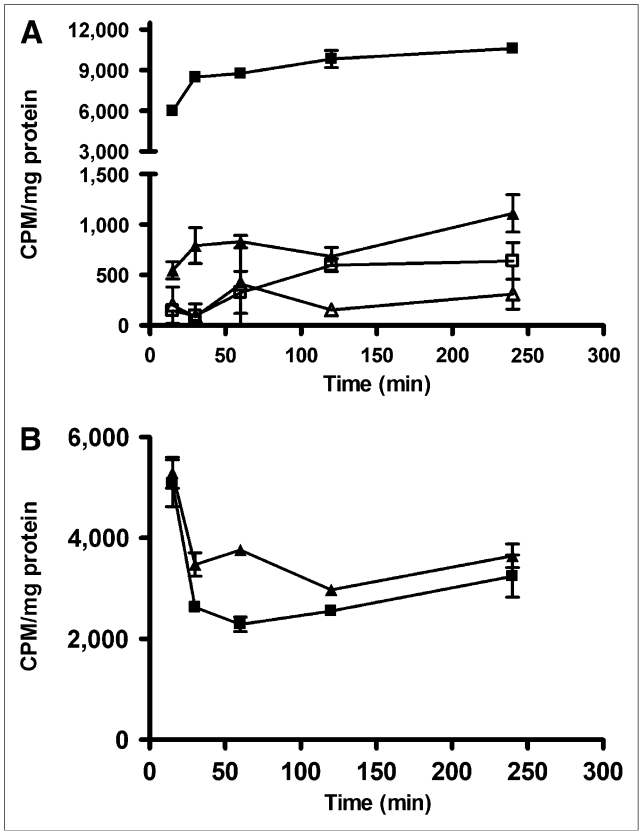

FIGURE 3. Results of internalization studies performed with ^{64}Cu-CB-TE2A-Y3-TATE (■) and ^{64}Cu-CB-TE2A-sst$_2$-ANT (▲) using SSTR-positive AR42J pancreatic tumor cells. Blocking studies were also performed using cold Y3-TATE (□) or cold sst$_2$-ANT (△), respectively. (A) Internalization results demonstrate that ^{64}Cu-CB-TE2A-Y3-TATE is internalized with greater efficiency than is ^{64}Cu-CB-TE2A-sst$_2$-ANT. Addition of blockade at each time point significantly reduces amount of radiopharmaceutical internalized and indicates that internalization is receptor-mediated process. (B) Amount of surface-bound activity removed from cells at all time points was also greater for ^{64}Cu-CB-TE2A-sst$_2$-ANT (▲) than for ^{64}Cu-CB-TE2A-Y3-TATE (■), indicating that less ^{64}Cu-CB-TE2A-sst$_2$-ANT was internalized over time course experiment. CPM = counts per minute.

http://jnm.snmjournals.org). In contrast, activity remained higher in the liver and kidneys, with slower clearance occurring from these tissues over time. From 1 to 24 h, activity in the liver fell by 35%, whereas 50% of the 1-h activity was excreted from the kidneys by 24 h. The amount of activity associated with SSTR-expressing tissues and AR42J tumors was also determined. Initial uptake in the tumor was modest when compared with the tracer uptake in the adrenals and pituitary gland. Over time, slow clearance from these tissues was also observed, with only 52% of the 1-h activity excreted from the adrenals at 24 h, whereas 60% and 69% of the 1-h activity had been cleared from the pituitary and tumor, respectively. This yielded tumor-to-blood ratios of 17, 42, and 20 at 1, 4, and 24 h, respectively, and tumor-to-muscle ratios of 40, 76, and 47 at 1, 4, and 24 h, respectively.

^{64}Cu-CB-TE2A-sst$_2$-ANT also demonstrated rapid blood clearance, and by 24 h after injection 95% of the 1-h activity had been filtered from the blood (Supplemental Table 2). However, unlike the former tracer, activity levels in the liver actually increased by 2% from the 1-h time point, whereas only 16% of the 1-h activity localized in the kidney was excreted by 24 h. Activity levels in SSTR-positive tissues and tumor were high, but clearance from these tissues was efficient, with 93% and 92% of the 1-h activity localized in the adrenal and pituitary glands excreted by 24 h, respectively. Finally, tumor uptake for this radiopharmaceutical was less than for the analogous ^{64}Cu-labeled agonist; however, clearance was slow, with only 50% of the 1-h activity being removed by 24 h. Tumor-to-blood ratios were 7, 35, and 72 at 1, 4, and 24 h, respectively, and tumor-to-muscle ratios were 17, 70, and 93 at 1, 4, and 24 h, respectively. Although the tumor uptake was lower for ^{64}Cu-CB-TE2A-sst$_2$-ANT, the tumor-to-background ratios were significantly higher than those of ^{64}Cu-CB-TE2A-Y3-TATE at 24 h (tumor-to-blood $P < 0.0001$; tumor-to-muscle $P < 0.0006$).

Blocking studies were performed at 4 h after injection for both radiotracers by coinjecting the cold peptide Y3-TATE or sst$_2$-ANT with its respective radiopharmaceutical (Fig. 5). Injection of Y3-TATE effectively blocked the binding of ^{64}Cu-CB-TE2A-Y3-TATE to the tumor by 75%, and coinjection of sst$_2$-ANT decreased the binding of ^{64}Cu-CB-TE2A-sst$_2$-ANT to AR42J tumors by 74%. This blocking resulted in 4-h tumor-to-blood and tumor-to-muscle ratios for ^{64}Cu-CB-TE2A-sst$_2$-ANT of 6 and 13, respectively. In addition, coinjection of the respective agonist or antagonist blockades also decreased the amount of activity observed in somatostatin-positive normal tissues. For example, coinjection of Y3-TATE with ^{64}Cu-CB-TE2A-Y3-TATE decreased the amount of activity observed in the pituitary and adrenal glands by 96% and 97%, respectively, whereas coadministration of sst$_2$-ANT with ^{64}Cu-CB-TE2A-sst$_2$-ANT blocked 70% and 86% of the activity in the pituitary and adrenal glands, respectively. However, tissues that were not SSTR-positive did not demonstrate reduced binding of the tracer.

In Vivo Small-Animal PET Imaging

Figure 6 represents the results of small-animal PET/CT imaging experiments performed on male Lewis rats bearing AR42J tumors in their hind limbs. Excellent tumor-to-background contrast is observed at 4 h after injection using ^{64}Cu-CB-TE2A-sst$_2$-ANT, with an average tumor SUV (n = 8) of 2.45 ± 0.5 and an SUV tumor-to-muscle ratio of 58. SUVs remained high even after 24 h, with the average tumor SUV (n = 6) decreasing by only 56% to 1.11 ± 0.24 and yielding an SUV tumor-to-muscle ratio of 37. These ratios are far better than those observed for ^{64}Cu-CB-TE2A-Y3-TATE, which had 4- and 24-h SUV tumor-to-muscle ratios of only 5 and 7, respectively (*10*). The effects of the administered blockade were also evident at 4 h. The average tumor SUV (n = 8) was calculated to be 0.62 ± 0.13, and the tumor-to-muscle ratio was calculated to be 10. Based on

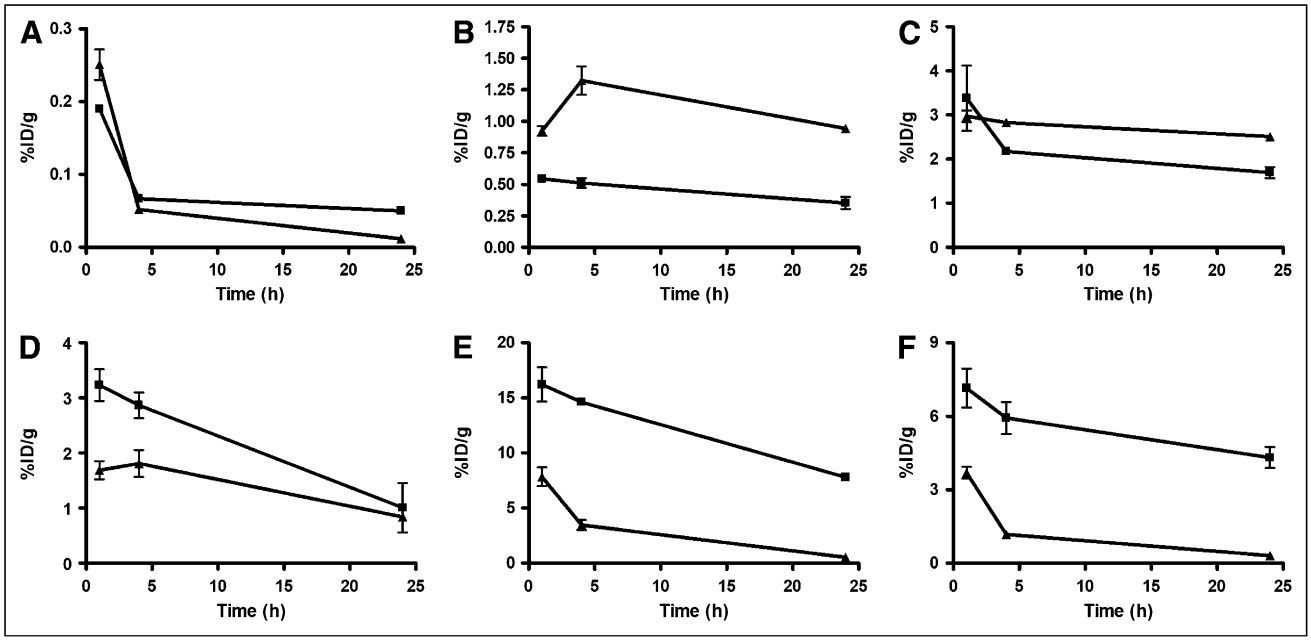

FIGURE 4. Biodistribution comparing clearance properties of ^{64}Cu-CB-TE2A-sst$_2$-ANT (▲) and ^{64}Cu-CB-TE2A-Y3-TATE (■) from blood (A), liver (B), kidney (C), tumor (D), adrenal glands (E), and pituitary gland (F). All data (n = 5; bars, ±SE) were decay-corrected. Note differences in y-axis scales. %ID = percentage injected dose.

SUV analysis, 75% of the tumor-associated activity was effectively blocked when excess sst$_2$-ANT was coinjected with the radiopharmaceutical, correlating well with the results of blocking studies performed during biodistribution experiments.

DISCUSSION

Recently, Ginj et al. reported a radiolabeled somatostatin peptide analog, ^{111}In-DOTA-sst$_2$-ANT, that demonstrated specificity for SSTR2 and high uptake in SSTR2-positive tumors in mice (*5*). Because of the impressive biodistribution of the ^{111}In-labeled sst$_2$-ANT, and the advantages of PET over SPECT in sensitivity and resolution, the goal of this work was to prepare a peptide–chelator conjugate using the peptide sst$_2$-ANT and the chelator CB-TE2A, label the conjugate with ^{64}Cu, and evaluate it as a PET radiopharmaceutical. ^{64}Cu was chosen as the PET isotope because of its favorable decay characteristics (half-life, 12.7 h; β^+, 17.8%, $E_{\beta+\ max}$, 656 keV; β^-, 38.4%, $E_{\beta-max}$, 573 keV), which make it useful for imaging and radiotherapy. The chelator CB-TE2A was chosen because of its ability to form ultrastable ^{64}Cu metal complexes. We chose to evaluate ^{64}Cu-CB-TE2A-sst$_2$-ANT in the AR42J model, because it is a model used to evaluate several radiometal-labeled somatostatin analogs (*10,19*).

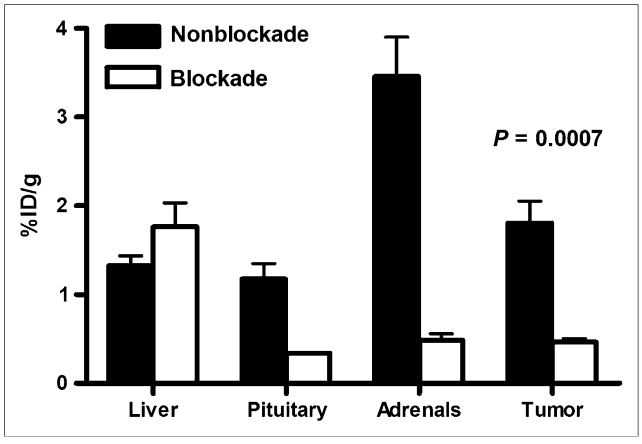

FIGURE 5. Tumor and SSTR-positive tissue labeling at 4 h after injection using ^{64}Cu-CB-TE2A-sst$_2$-ANT without blockade and at 4 h after injection when coinjected with sst$_2$-ANT as blocking agent. Decrease in affinity by radiopharmaceutical for tumor and SSTR-positive tissues is evident, suggesting that interaction of radiotracer with these tissues is receptor-mediated process. %ID = percentage injected dose.

^{64}Cu-CB-TE2A-sst$_2$-ANT demonstrated a K_d of 26 nM and a B_{max} of 23,000 fmol/mg for the SSTR2 with AR42J rat pancreatic carcinoma cell membranes. These values stand in contrast to those determined for ^{64}Cu-CB-TE2A-Y3-TATE, which should function as an agonist for the SSTR2. Under similar experimental conditions, ^{64}Cu-CB-TE2A-Y3-TATE demonstrated a K_d of 1.5 nM and a B_{max} of 1,551 fmol/mg (*10*). These results suggest that although the sst$_2$-ANT peptide does not have as high a binding affinity for the SSTR2 receptor, it is able to label approximately 14-fold more sites on the membrane than the Y3-TATE compound and is in agreement with what Ginj et al. observed in comparing ^{111}In-DOTA-sst$_2$-ANT with the agonist ^{111}In-DTPA-TATE (*5*). This increase in B_{max} may be attributed to the ability of the antagonist to interact and bind to a larger number of SSTR2 conformations and possibly its

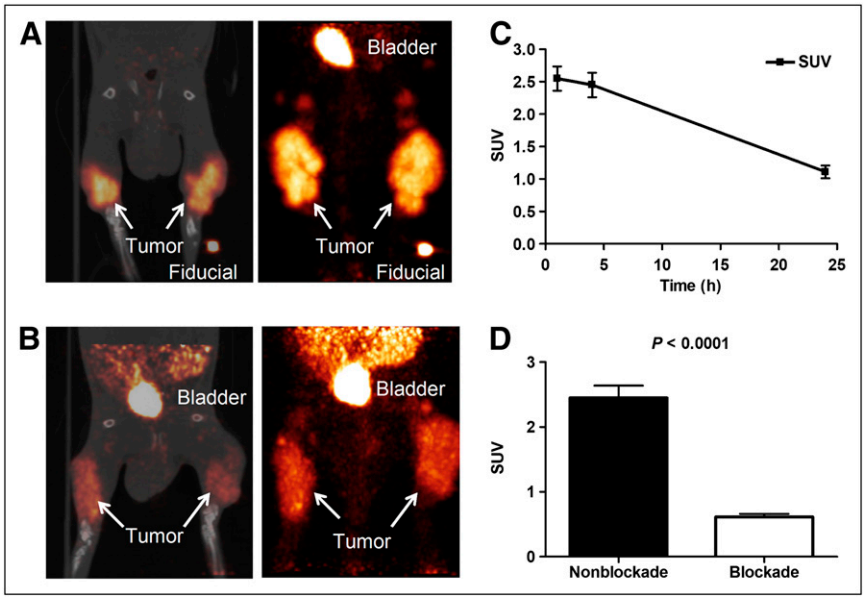

FIGURE 6. (A) Representative small-animal PET image at 4 h of rat injected with ^{64}Cu-CB-TE2A-sst$_2$-ANT. Left image is representative slice from small-animal PET/CT fusion image and right image is small-animal PET projection view of same animal. Calculated SUV for the tumor in left hind limb was determined to be 2.7 and SUV for tumor in right hind limb was determined to be 2.8. (B) Representative small-animal PET image at 4 h of rat injected with ^{64}Cu-CB-TE2A-sst$_2$-ANT and sst$_2$-ANT as blocking agent. Left image is representative slice from small-animal PET/CT fusion image and right image is small-animal PET projection view of same animal. In animal receiving blockade, SUV for tumor in left hind limb was calculated to be 0.74 and SUV for tumor in right hind limb was calculated to be 0.51. (C) Graphical plot of change in average SUV over time. Even after 24 h, SUV remains high, suggesting enhanced binding of ^{64}Cu-CB-TE2A-sst$_2$-ANT for SST$_2$ receptor. (D) Graphical representation that demonstrates change in observed SUV when excess cold sst$_2$-ANT is coinjected with radiopharmaceutical, indicating that binding of radiopharmaceutical to SSTR-positive tumor is receptor-mediated.

stabilization in the lipid-rich environment of the receptor (*5*). Although AR42J tumor cells have also been shown to express SSTR1, SSTR3, and SSTR5, the affinity of these receptor subtypes for sst$_2$-ANT is 100 times lower than its affinity for SSTR2 (*20*), suggesting that binding to other subtypes does not significantly interfere with these binding results.

Assays were performed to determine the extent of radiopharmaceutical internalization induced when ^{64}Cu-CB-TE2A-sst$_2$-ANT was incubated with AR42J cells and data were compared with the radiolabeled agonist ^{64}Cu-CB-TE2A-Y3-TATE. Rapid internalization of ^{64}Cu-CB-TE2A-Y3-TATE by AR42J tumor cells was observed between 15 and 30 min. This rapid internalization is followed by a slow rise in the amount of activity internalized after 30 min, suggesting that after 30 min have elapsed, receptor saturation has been achieved. At 30 min, it is likely that receptors that have bound the radiopharmaceutical have been internalized, and few receptors are available on the cell surface to bind more of the radiopharmaceutical, which may explain why internalization after 30 min remains a relatively static process. Internalization of ^{64}Cu-CB-TE2A-Y3-TATE was blocked with excess Y3-TATE, demonstrating this to be a receptor-mediated process. Much lower, yet significant, levels of internalization were observed for ^{64}Cu-CB-TE2A-sst$_2$-ANT. Similar to ^{64}Cu-CB-TE2A-Y3-TATE, internalization of ^{64}Cu-CB-TE2A-sst$_2$-ANT occurred rapidly until 30 min but slowed after this time point. Cell surface–associated activity was greater for ^{64}Cu-CB-TE2A-sst$_2$-ANT than for ^{64}Cu-CB-TE2A-Y3-TATE after 30 min, suggesting that internalization occurs less rapidly for the former and may reflect the labeling of an increased number of binding sites on the cell surface.

These observations stand in contrast to what has been previously reported, as Ginj et al. showed no observable internalization of the sst$_2$-ANT peptide receptor complex when immunofluorescence microscopy was used to study the effect of agonists and antagonists on HEK229 cells, which were stably transfected to express SSTR2 (*5*). Reubi et al. have demonstrated that relatively small changes in a radiolabeled peptide, such as changing the chelator, can markedly change the SSTR binding profile of the somatostatin analogs (*21*). These small changes may have proven sufficient to alter the characteristics of the peptide and may explain why low yet significant levels of internalization of ^{64}Cu-CB-TE2A-sst$_2$-ANT are observed. In addition, previously reported analyses used fluorescence microscopy to determine the extent of receptor internalization. Although providing valuable information, fluorescence microscopy remains a qualitative assay when compared with assays with radiolabeled compounds (*22*). Finally, because this work was concerned with the internalization of the radiopharmaceutical and not merely the receptor, membrane remodeling must also be considered. The plasma membrane of a eukaryotic cell is a dynamic structure, and substantial amounts of the plasma membrane are being continually recycled (*23*). This recycling allows membrane components and those ligands associated either specifically or nonspecifically with the membrane to be brought into the interior of the cell through mechanisms other than receptor-mediated endocytosis.

Comparative in vivo studies of ^{64}Cu-CB-TE2A-sst$_2$-ANT and ^{64}Cu-CB-TE2A-Y3-TATE were performed. Although the biodistribution of ^{64}Cu-CB-TE2A-Y3-TATE has been determined previously, it was reevaluated for a more accurate

comparison with ^{64}Cu-CB-TE2A-sst$_2$-ANT. In the previous study, 2-fold more activity and 3-fold more mass were injected per animal than in the current study (*10*), possibly giving rise to higher uptake in the AR42J tumors (*24*).

Both radiopharmaceuticals demonstrated rapid blood clearance at all time points, indicating that this tracer is stable after injection, but liver and kidney clearance were more modest over time. This slower clearance in the liver can be attributed to a main excretion route, and uptake and clearance in the kidneys are slower because of an expected +1 charge on the radiopharmaceutical. Several reports have been published describing the effect of radiopharmaceutical charge on kidney uptake. Studies using ^{111}In-DTPA–conjugated peptides demonstrated that renal retention was highest for positively charged peptide conjugates, and similar charge effects were seen when ^{64}Cu-labeled azamacrocycles were studied (*25,26*). In addition, similar trends were also observed for ^{64}Cu-CB-TE2A-Y3-TATE when previously evaluated (*10*). Both radiotracers also demonstrated substantial uptake in SSTR-positive tissues and AR42J tumors, which was reduced on the coinjection of blockade, indicating that interaction between the radiopharmaceuticals and the tissues is a receptor-mediated process. Although ^{64}Cu-CB-TE2A-sst$_2$-ANT demonstrated lower uptake in SSTR-positive tissues and tumor than did ^{64}Cu-CB-TE2A-Y3-TATE, ^{64}Cu-CB-TE2A-sst$_2$-ANT demonstrated higher tumor-to-blood and tumor-to-muscle ratios at the latest time point of 24 h. These results may be a reflection of the increased chemical stability and increased hydrophobicity of the antagonist, which results in a longer duration of action and possible stabilization in the lipid-rich environment of the receptors (*5*). In addition, rebinding of ^{64}Cu-CB-TE2A-sst$_2$-ANT after dissociation from the receptor also may explain these higher ratios and the superior tumor-to-background contrast observed in small-animal imaging experiments (*27*). This observation suggests that ^{64}Cu-CB-TE2A-sst$_2$-ANT, compared with ^{64}Cu-CB-TE2A-Y3-TATE, seems to remain bound to the tumor tissue for an increased length of time and provides insight into the promise of ^{64}Cu-CB-TE2A-sst$_2$-ANT as a PET agent.

The relative tumor uptake observed in our experiments is much lower than what was reported by Ginj et al. with HEK229 cells that were stably transfected to express SSTR2 and ^{111}In-DOTA-sst$_2$-ANT (*5*). In this study, the rat pancreatic carcinoma cell line AR42J reflects a tumor cell line with a natural expression of SSTR2 and other somatostatin subtypes (*20*). Hence, the concentration of SSTR2 in AR42J cells is lower than the SSTR2 number on the engineered HEK229 cells, accounting for the discrepancy in the biodistribution results of the 2 reports (*5*). Moreover, somatostatin receptor number on normal SSTR-positive tissues has been observed to be species-dependant, possibly explaining differences in radiopharmaceutical uptake between this report and the report published by Ginj et al. For example, Ludvigsen et al. observed higher SSTR2 expression in the pancreas of mice than in the pancreas of normal rats (*28*). Questions arise as to whether these results observed by Ginj et al. in a SSTR2-transfected cell line are an accurate reflection of the behavior of sst$_2$-ANT in vivo, and the data presented here offer another perspective on imaging SSTR2 with radiolabeled antagonists. Despite the lower tumor uptake, small-animal imaging of AR42J tumors with ^{64}Cu-CB-TE2A-sst$_2$-ANT produced images with good tumor-to-background contrast and high SUVs for target tissues (Fig. 6). Both contrast and SUVs were decreased by the coadministration of blockade (sst$_2$-ANT), demonstrating that binding of the radiopharmaceutical to the tumor in vivo is a receptor-mediated process and correlates with similar observations obtained through biodistribution studies.

CONCLUSION

The PET radiopharmaceutical ^{64}Cu-CB-TE2A-sst$_2$-ANT has been evaluated in vitro using receptor binding and internalization assays and in vivo using biodistribution and small-animal imaging experiments with a natively SSTR2-expressing cell line, AR42J. Despite having a lower affinity for the SSTR2 receptor than the agonist ^{64}Cu-CB-TE2A-Y3-TATE and relatively modest tumor uptake, ^{64}Cu-CB-TE2A-sst$_2$-ANT had superior tumor-to-background contrast, resulting in high tumor SUVs even after 24 h. ^{64}Cu-CB-TE2A-sst$_2$-ANT is an attractive agent, worthy of future study as a PET radiopharmaceutical for the imaging of somatostatin receptor–positive tumors.

ACKNOWLEDGMENTS

We thank Lori Strong, Ann Stroncek, and Jerrel Rutlin for technical assistance. Funding for this research was provided by National Cancer Institute (NCI) grants R01 CA064475 and F32 CA115148 and National Institutes of Health (NIH) grant R01 EB 1430. The production of ^{64}Cu at Washington University School of Medicine was supported by NCI grant R24 CA86307. Small-animal imaging at Washington University School of Medicine was supported by NIH grant 5 R24 CA83060.

REFERENCES

1. Rogers BE, McLean SF, Kirkman RL, et al. In vivo localization of [^{111}In]-DTPA-D-Phe1-octreotide to human ovarian tumor xenografts induced to express the somatostatin receptor subtype 2 using an adenoviral vector. *Clin Cancer Res.* 1999;5:383–393.
2. Anderson CJ, Dehdashti F, Cutler PD, et al. ^{64}Cu-TETA-octreotide as a PET imaging agent for patients with neuroendocrine tumors. *J Nucl Med.* 2001;42:213–221.
3. Li WP, Meyer LA, Anderson CJ. Radiopharmaceuticals for positron emission tomography imaging of somatostatin receptor positive tumors. *Top Curr Chem.* 2005;252:179–192.
4. Edwards WB, Xu B, Akers W, et al. Agonist-antagonist dilemma in molecular imaging: evaluation of a monomolecular multimodal imaging agent for the somatostatin receptor. *Bioconjug Chem.* 2008;19:192–200.
5. Ginj M, Zhang H, Waser B, et al. Radiolabeled somatostatin receptor antagonists are preferable to agonists for in vivo peptide receptor targeting of tumors. *Proc Natl Acad Sci USA.* 2006;103:16436–16441.

6. Wadas TJ, Wong EH, Weisman GR, Anderson CJ. Copper chelation chemistry and its role in copper radiopharmaceuticals. *Curr Pharm Des.* 2007;13:3–16.
7. Hubin TJ, McCormick JM, Collinson SR, Alcock NW, Busch DH. Ultra rigid cross-bridged tetraazamacrocycles as ligands: the challenge and the solution. *J Chem Soc Chem Commun.* 1998;16:1675–1676.
8. Weisman GR, Rogers ME, Wong EH, Jasinski JP, Paight ES. Cross-bridged cyclam: protonation and Li+ complexation in a diamond-lattice cleft. *J Am Chem Soc.* 1990;112:8604–8605.
9. Boswell CA, Sun X, Niu W, et al. Comparative in vivo stability of copper-64-labeled cross-bridged and conventional tetraazamacrocyclic complexes. *J Med Chem.* 2004;47:1465–1474.
10. Sprague JE, Peng Y, Sun X, et al. Preparation and biological evaluation of copper-64-labeled Tyr3-octreotate using a cross-bridged macrocyclic chelator. *Clin Cancer Res.* 2004;10:8674–8682.
11. Qaim SM, Bisinger T, Hilgers K, Nayak D, Coenen HH. Positron emission intensities in the decay of ^{64}Cu, ^{76}Br and ^{124}I. *Radiochim Acta.* 2007;95:67–73.
12. McCarthy DW, Shefer RE, Klinkowstein RE, et al. The efficient production of high specific activity Cu-64 using a biomedical cyclotron. *Nucl Med Biol.* 1997;24:35–43.
13. Achilefu S, Wilhelm RR, Jimenez HN, Schmidt MA, Srinivasan A. A new method for the synthesis of tri-tert-butyl diethylenetriaminepentaacetic acid and its derivatives. *J Org Chem.* 2000;65:1562–1565.
14. Achilefu S, Jimenez HN, Dorshow RB, et al. Synthesis, in vitro receptor binding and in vivo evaluation of fluorescein and carbocyanine peptide-based optical contrast agents. *J Med Chem.* 2002;45:2003–2015.
15. Wadas TJ, Anderson CJ. Radiolabeling of TETA- and CB-TE2A-conjugated peptides with copper-64. *Nat Protoc.* 2006;1:3062–3068.
16. Anderson CJ, Jones LA, Bass LA, et al. Radiotherapy, toxicity and dosimetry of copper-64-TETA-octreotide in tumor-bearing rats. *J Nucl Med.* 1998;39:1944–1951.
17. Wang M, Caruano AL, Lewis MR, Meyer LM, VanderWaal RP, Anderson CJ. Subcellular localization of radiolabeled somatostatin analogues: implications for targeted radiotherapy of cancer. *Cancer Res.* 2003;63:6864–6869.
18. Lewis JS, Srinivasan A, Schmidt MA, Anderson CJ. In vitro and in vivo evaluation of ^{64}Cu-TETA-Tyr^3-octreotate: a new somatostatin analog with improved target tissue uptake. *Nucl Med Biol.* 1999;26:267–273.
19. Decristoforo C, Melendez-Alafort L, Sosabowski JK, Mather SJ. ^{99m}Tc-HYNIC-[Tyr3]-octreotide for imaging somatostatin-receptor-positive tumors: preclinical evaluation and comparison with ^{111}In-octreotide. *J Nucl Med.* 2000;41:1114–1119.
20. Hofsli E, Thommesen L, Norsett K, et al. Expression of chromogranin A and somatostatin receptors in pancreatic AR42J Cells. *Mol Cell Endocrinol.* 2002; 194:165–173.
21. Reubi JC, Schar J-C, Waser B, et al. Affinity profiles for human somatostatin receptor subtypes SST1-SST5 of somatostatin radiotracers selected for scintigraphic and radiotherapeutic use. *Eur J Nucl Med.* 2000;27:273–282.
22. Liu Q, Cescato R, Dewi DA, Rivier J, Reubi JC, Schonbrunn A. Receptor signaling and endocytosis are differentially regulated by somatostatin analogs. *Mol Pharmacol.* 2005;68:90–101.
23. Cohn J. Vasoactive intestinal peptide stimulates protein phosphorylation in a colonic epithelial cell line. *Am J Physiol.* 1987;16:G420–G424.
24. Breeman WAP, de Jong M, Bernard B, et al. Tissue distribution and metabolism of radioiodinated DTPA(0), D-Tyr(1) and Tyr(3) derivatives of octreotide in rats. *Anticancer Res.* 1998;18:83–89.
25. Akizawa H, Arano Y, Mifune M, et al. Effect of molecular charges on renal uptake of ^{111}In-DTPA-conjugated peptides. *Nucl Med Biol.* 2001;28:761–768.
26. Jones-Wilson TM, Deal KA, Anderson CJ, et al. The *in vivo* behavior of copper-64-labeled azamacrocyclic compounds. *Nucl Med Biol.* 1998;25:523–530.
27. Ginj M, Zhang H, Eisenwiener K, et al. New pansomatostatin ligands and their chelated versions: affinity, profile, agonist activity, internalization, and tumor targeting. *Clin Cancer Res.* 2008;14:2019–2027.
28. Ludvigsen E, Olsson R, Stridsberg M, Janson ET, Sandler S. Expression and distribution of somatostatin receptor subtypes in the pancreatic islets of mice and rats. *J Histochem Cytochem.* 2004;52:391–400.